Heliyon 10 (2024) e26443

Contents lists available at ScienceDirect

Heliyon

journal homepage: www.cell.com/heliyon

Research article

Removal of phenol from wastewater using *Luffa cylindrica* fibers in a packed bed column: Optimization, isotherm and kinetic studies

Samuel Ogunniyi [a], Ebuka Chizitere Emenike [b,*], Kingsley O. Iwuozor [b], Joshua O. Ighalo [c,d], Abdelrahman O. Ezzat [e], Tunmise Latifat Adewoye [a], Abel Egbemhenghe [f,g], Hussein K. Okoro [h], Adewale George Adeniyi [a,i,**]

[a] *Department of Chemical Engineering, University of Ilorin, P. M. B. 1515, Ilorin, Nigeria*
[b] *Department of Pure and Industrial Chemistry, Nnamdi Azikiwe University, P. M. B. 5025, Awka, Nigeria*
[c] *Department of Chemical Engineering, Nnamdi Azikiwe University, P. M. B. 5025, Awka, Nigeria*
[d] *Department of Chemical Engineering, Kansas State University, Manhattan, KS, USA*
[e] *Department of Chemistry, College of Sciences, King Saud University, Riyadh, 11451, Saudi Arabia*
[f] *Department of Chemistry and Biochemistry, College of Art and Science, Texas Tech University, USA*
[g] *Department of Chemistry, Lagos State University, Ojo, Lagos, Nigeria*
[h] *Environmental-Analytical Research Group, Department of Industrial Chemistry, Faculty of Physical Sciences, University of Ilorin, P. M. B. 1515, Ilorin, Nigeria*
[i] *Department of Chemical Engineering, College of Engineering and Technology, Landmark University, Omu-aran, Nigeria*

ARTICLE INFO

Keywords:
Phenol adsorption
Luffa cylindrica fiber
Packed bed
Equilibrium modeling

ABSTRACT

This research entails a comparison of the effectiveness of unmodified *Luffa cylindrica* fiber in a fully packed bed (RLCF) and NaOH-modified *Luffa cylindrica* fiber in another fully packed bed (MLCF) in the context of phenol removal from wastewater. Experimental data obtained through batch adsorption experiments were utilized to determine the most suitable model. It was observed that as the initial concentration of phenol increased from 100 to 500 mg/l, the maximum percentage removal increased from 63.5 to 83.1% for RLCF-PB and from 89.9 to 99.5% for MLCF-PB. The correlation coefficient (R^2) was calculated for the Langmuir, Freundlich, Temkin, Harkin-Jura, Halsey, and Flory-Huggins models for both materials. The analysis revealed that the pseudo-second-order model was the most suitable, followed by the Elovich model, with the pseudo-first-order model being the least suitable. The Weber-Morris diffusion model suggested that pore diffusion was the rate-determining step, and diffusion at the border layer was determined to be endothermic, feasible, heterogeneous, and spontaneous. In summary, this study indicates that MLCF-PB is a promising material for the efficient removal of phenol from aqueous solutions.

1. Introduction

Releasing untreated wastewater into the environment poses a major threat to both human health and the ecosystem. The effects of untreated wastewater can be severe and wide-ranging, impacting not only human health but also the environment and the economy [1,

* Corresponding author.
** Corresponding author. Department of Chemical Engineering, University of Ilorin, P. M. B. 1515, Ilorin, Nigeria.
E-mail addresses: emenikechizitere@gmail.com (E.C. Emenike), adeniyi.ag@unilorin.edu.ng (A.G. Adeniyi).

https://doi.org/10.1016/j.heliyon.2024.e26443
Received 9 August 2023; Received in revised form 11 February 2024; Accepted 13 February 2024
Available online 17 February 2024

2]. There has been an increasing awareness in recent times of the consequences of water pollution and the need for effective management strategies to prevent contamination and ensure the safety of our water supply [3–5]. One of the major pollutants commonly found in wastewater is phenol, which is a toxic and hazardous organic compound.

Phenol is a common water contaminant that can have significant impacts on individual well-being and the environment. It is commonly present in industrial effluents from chemical, petrochemical, and pharmaceutical industries, where it is used in the production of plastics, resins, and other industrial chemicals [6–8]. While phenol is not considered a major water pollutant, it becomes toxic and dangerous when present in water at elevated levels [9]. Consumption of food or drink that contains elevated levels of phenol can pose a serious health risk, particularly for vulnerable populations such as children and the elderly. These health implications of phenol include respiratory irritation, skin burns, and even death in extreme cases [10,11]. It can also have harmful effects on aquatic ecosystems, such as killing fish and other aquatic life [12]. The importance of monitoring and controlling phenol levels in water is therefore critical.

Numerous techniques have been created to eliminate phenol from wastewater, including coagulation, biological treatment, oxidation, and adsorption. The adsorption method is often preferred because of its ease of use, efficiency, and affordability [13,14]. The potential of using adsorbents like activated carbon, zeolites, and natural fibers to eliminate phenol from wastewater has been explored. Among these, natural fibers are particularly attractive due to their high availability, low cost, and biodegradability [15].

Luffa cylindrica fibers (LCF) are a natural fiber that has shown potential as an adsorbent for phenol removal. *Luffa cylindrica* is a Cucurbitaceae plant species that is native to tropical regions [16]. It is composed of lignocellulosic biomass that contains cellulose, hemicellulose, and lignin. Due to its fibrous structure, it possesses a high surface area and pore volume, which make it a feasible option for phenol adsorption [17]. Previous studies have shown that LCF can be used to remove various pollutants from wastewater, including dyes [18], heavy metals [19], and organic compounds [20,21], among others. However, limited research has focused on their potential for phenol removal from wastewater. Furthermore, there are some limitations on using agricultural residue as an adsorbent for phenol uptake from water, such as its requirement for pre-treatment before use to remove impurities and ensure optimal adsorption capacity [22–24]. While treatment of the biosorbents with chemicals can potentially enhance their adsorption capacity and efficiency, it may result in the production of even more dangerous by-products.

In this study, we investigate the potential of raw and modified LCF to remove phenol from wastewater. Raw *Luffa cylindrica fibers* (RLCF) were used as a reference material, while modified *Luffa cylindrica fibers* (MLCF) were treated with NaOH to enhance their adsorption capacity. The ability to select the most effective adsorbent for the removal of a specific contaminant from water is one of the major challenges facing the adsorption process. Nonetheless, it is crucial to assess the viability and appropriateness of a cheap, renewable material for addressing the threat of phenol contamination. Herein, the adsorption of phenol onto RLCF and MLCF was carried out in a fully packed bed to simulate the practical application of these materials. The present investigation adds to the existing knowledge on the utilization of natural fibers as an adsorbent for treating wastewater.

2. Methodology

2.1. Materials

Luffa cylindrica pods were sourced from a farm in Ilorin, Nigeria. The chemical activator employed in this work was analytical-grade sodium hydroxide (Sigma Aldrich), which was obtained from a local market.

2.2. Adsorbent preparation

The *Luffa cylindrica* pods were gathered, and the sponges underneath were meticulously removed, rinsed with distilled water, and dried at 80 °C to get rid of any residual moisture. They were split into similar parts and stored for subsequent analysis. The sample was labeled raw *Luffa cylindrica* fibers (RLCF). For the pre-treatment, samples of the fibers were soaked in a 5% solution of sodium hydroxide and allowed to stay on the bench for 24 h. The fibers were then washed and rinsed with distilled water at room temperature until they reached a neutral pH. They were then oven-dried to a consistent weight at 105 °C. The resulting NaOH-modified *Luffa cylindrica* fibers (MLCF) were stored in the desiccator for the adsorption experiment. The modification with NaOH because prior research has demonstrated its ability to enhance fiber wettability, break down cellulose molecules, and boost fiber surface roughness [16].

2.3. Adsorbent characterization

The characteristics of both RLCF and MLCF were established through the use of Fourier transform infrared (FTIR) and scanning electron microscopy coupled with energy dispersive X-ray spectroscopy (SEM-EDX). The FTIR (Shimadzu FTIR-8400S instrument, Japan) was employed to identify the functional groups within the materials. On the other hand, SEM-EDX (Phenom ProX, Phenom-World BV, Netherlands) was utilized to determine the morphology and elemental composition of the adsorbents.

2.4. Preparation of adsorbate

Phenol (99.9% purity, Aldrich) was used as an adsorbate. 1.0 g of phenol were solubilized in 1 L of distilled water to produce a stock concentration of 1000 mg/l. Diluted stock solutions using distilled water were used to make the experimental solutions in a series of

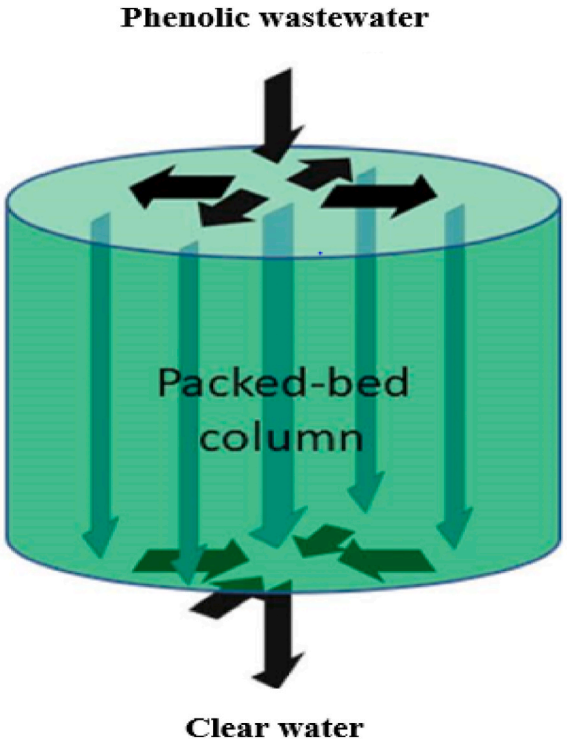

Fig. 1. Schematic diagram of the filter bed.

steps to get the desired concentrations (100–500 mg/l) for batch equilibrium experiments.

2.5. Construction of a packed bed

The filter bed was made from a 1.3 dm^3 polypropylene (PP) plastic jar with an opening valve at the base for sample collection and an openable lid at the top for simulated wastewater (phenolic wastewater) entry flow. A diagrammatic representation of the filter bed is presented in Fig. 1. Both the untreated and treated fibres had a 0.075 packing factor in each packed bed. This is the greatest packing that could be achieved [25].

2.6. Adsorption experiments

Batch adsorption studies in a number of packed beds were conducted to measure the effectiveness of phenol adsorption onto LCF (1300 cm^3). Each column was packed with LCF and initially contained 13 g of adsorbents and 100 mL of solutions with varying concentrations (ranging from 100 to 500 mg/l). A mechanical rotary shaker was used at 200 rpm until equilibrium was attained after 4 h. To reach maximum equilibrium, a time contact equal to 240 min was fixed for all experiments. The effluent concentrations of the samples were examined using a UV/Vis spectrophotometer (UV-6100A) at 270 nm. Eqn. 1 was used to calculate the adsorbent's adsorbed capacity to phenol, and the removal efficiency was calculated using Eqn. (2):

$$Adsorption\ capacity\ (q_e) = (C_O - C_e)\frac{V}{M} \tag{1}$$

$$Removal\ Efficency\ (\%) = \frac{(C_O - C_e)}{C_O} * 100 \tag{2}$$

Where the initial and equilibrium phenol concentrations (mg/l) are represented by C_o and C_e, respectively. The dry mass of added adsorbent is M (g), and the aqueous solution's volume is V (l).

2.7. Studies on adsorption isotherms

Six different models (Langmuir, Freundlich, Temkin, Harkins Jura, Halsey, and Flory-Huggins) were utilized to fit the adsorption data; the best fit for this investigation was determined by calculating the constants of these models. The R^2 value was also computed to indicate the level of relationship between the experimental data and the predicted values. The expressions for the linear forms of

Langmuir, Freundlich, Temkin, Harkins Jura, Halsey, and Flory-Huggins are given in **Eqns.** 3-8. From the plot of $\frac{C_e}{q_e}$ against C_e, the Langmuir constants K_L, R_L, and q_{max} were calculated. A dimensionless equilibrium unit can be used to express the main essence of the Langmuir model (R_L). The constants K_F and 1/n for the Freundlich model were obtained by plotting $\log q_e$ against $\log C_e$. For the Temkin and Harkins Jura models, the constants A and B were gotten from the linear graph of q_e against $\ln C_e$ and $\frac{1}{q_e^2}$ against $\log C_e$, respectively. The Halsey constants K and 1/n were derived from the graph of $\ln q_e$ against $\ln C_e$, and the Flory-Huggins constants, K_{FH} and n_{FH} were obtained when $\ln \frac{\theta}{C_O}$ was plotted against $\ln(1-\theta)$.

$$\frac{C_e}{q_e} = \frac{1}{q_m} C_e + \frac{1}{q_m K_L} \tag{3}$$

$$\log q_e = \frac{1}{n} \log C_e + \log K_f \tag{4}$$

$$q_e = B \ln C_e + B \ln A_T \tag{5}$$

$$\frac{1}{q_e^2} = \frac{B}{A} - \frac{1}{A} \log C_e \tag{6}$$

$$\ln q_e = \frac{1}{n} \ln K - \frac{1}{n} \ln C_e \tag{7}$$

$$\ln \frac{\theta}{C_O} = n \ln(1-\theta) + \ln(1-\theta) \tag{8}$$

Where the equilibrium adsorption capacity is q_e, K_L is the free energy (L/mg), the maximal adsorption capacity (mg/g) at monolayer coverage is given by q_m, K_f and n are the Freundlich constants, A and B are the Temkin constants, and θ denotes the number of adsorbates occupying sorption sites.

2.8. Adsorption kinetics studies

In order to learn more about probable rate-controlling processes and adsorption mechanisms, the kinetics were analyzed using pseudo-first-order (PFO) **(Eqn. (9))**, pseudo-second-order (PSO) (**Eqn. (10)**), and Elovich models (**Eqn. (11)**). Their linear plots were determined using **Eqns. (9)–(11)**. The performance of the adsorption process was predicted using all of the factors derived from the plots.

$$\ln(q_e - q_t) = \ln q_e - K_1 t \tag{9}$$

$$\frac{t}{q(t)} = \frac{1}{K_2 q_e^2} + \frac{t}{q_e} \tag{10}$$

$$q_t = \left(\frac{1}{\beta}\right) \ln t + \left(\frac{1}{\beta}\right) \ln \alpha\beta \tag{11}$$

2.9. Test of the kinetics model

The accuracy of the kinetic models is evaluated by the combination of the sum of squared errors (SSE) and the average relative error (ARE). In addition to determining the R^2 value, the reliability of both kinetic models was verified by analyzing the SSE and ARE. The adsorption kinetics of phenol onto raw *Luffa cylindrica* fiber-packed beds (RLCF-PB) and modified *Luffa cylindrica* fiber-packed beds (MLCF-PB) were tested at varying concentrations. The effectiveness of the model was evaluated using **Eqn. (12)** and **13** as shown below.

$$SSE = \sum_{i=1}^{n} \frac{\left(q_{e,cal} - q_{e,exp}\right)^2}{n} \tag{12}$$

$$ARE = \frac{100}{n} \sum_{i=1}^{n} \left(\frac{q_{e,exp} - q_{e,cal}}{q_{e,exp}} \right) \tag{13}$$

Where $q_{e,cal}$ is the sorption capacity calculated at equilibrium (mg/g), $q_{e,exp}$ is the experimental equilibrium sorption capacity (mg/g), and n denotes the total number of experimental data points.

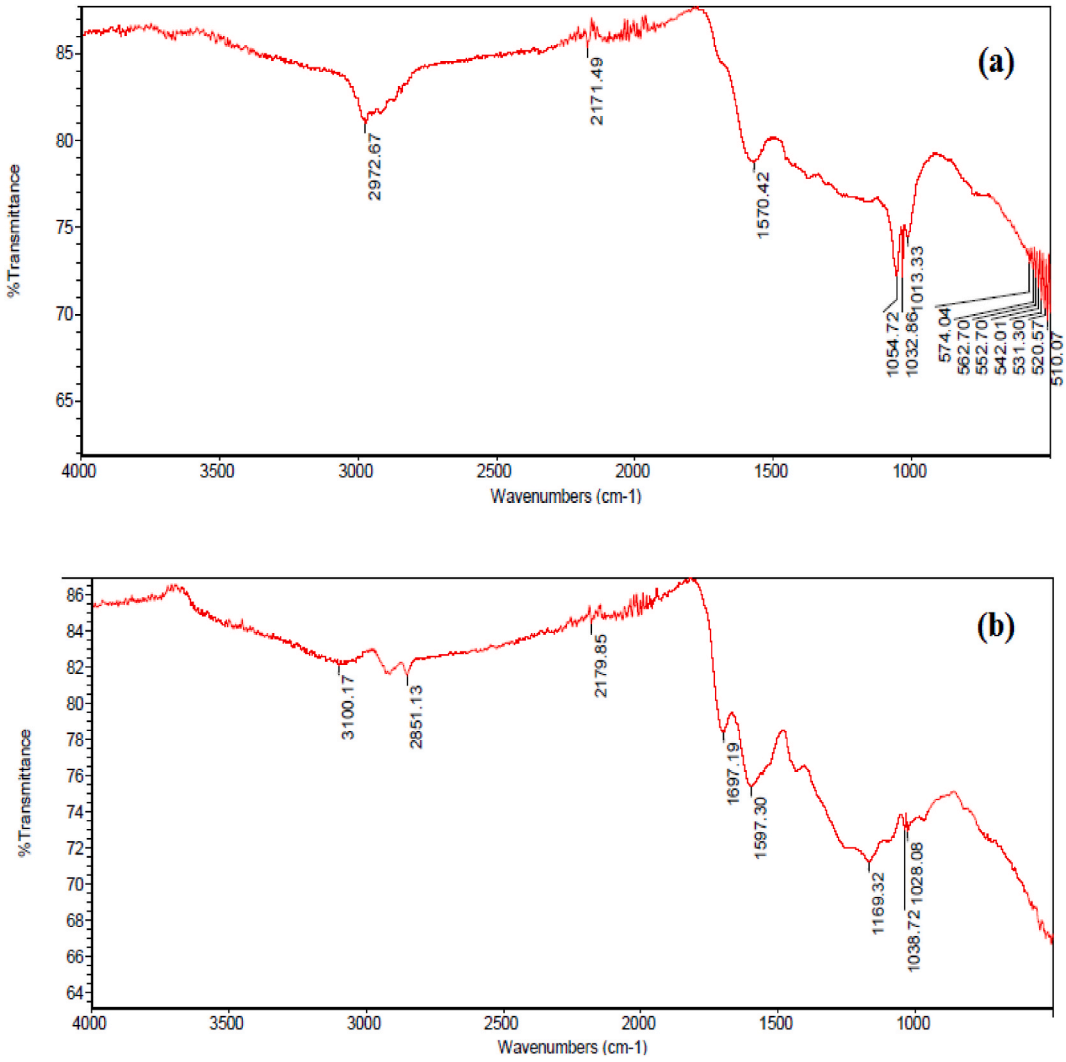

Fig. 2. FTIR spectra of (a) RLCF and (b) MLCF.

2.10. Adsorption thermodynamic

The thermodynamic characteristics of phenol adsorption onto RLCF-PB and MLCF-PB were determined through analysis of experimental data at various temperatures. The data were used to determine thermodynamic parameters like entropy (ΔS°), Gibbs energy (ΔG°), and enthalpy change (ΔH°). The volume of the phenolic solution (300 mg/l), dosages (13 g), and agitation speed (200 rpm) were unaltered. The temperature range of 40–60 °C at 10–60 min was used. The treated effluents were withdrawn and tested with a UV/Vis spectrophotometer according to the design. ΔS° and ΔH° were determined by plotting ΔG° against temperatures. The equilibrium constant K_d was determined using Eqn. (14) and 15

$$\Delta G^{O} = -RT \ln K_d \tag{14}$$

$$\Delta G^{O} = \Delta H^{O} - T\Delta S \tag{15}$$

Combining Eqn. (14) & 15 gave Eqn. 16

$$\ln K_d = \frac{\Delta H}{R} \times \frac{1}{T} - \frac{\Delta S}{R} \tag{16}$$

R (8.314 J/mol K) represents the gas constant, T (K) represents the temperature (absolute), and K_d is the equilibrium constant.

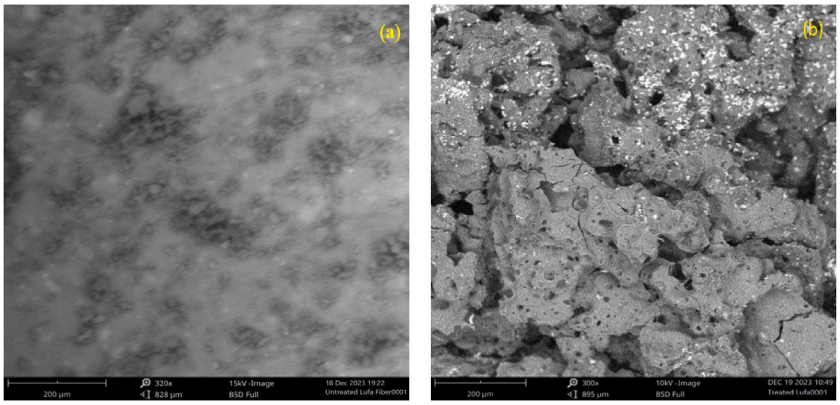

Fig. 3. SEM images of (a) RLCF and (b) MLCF.

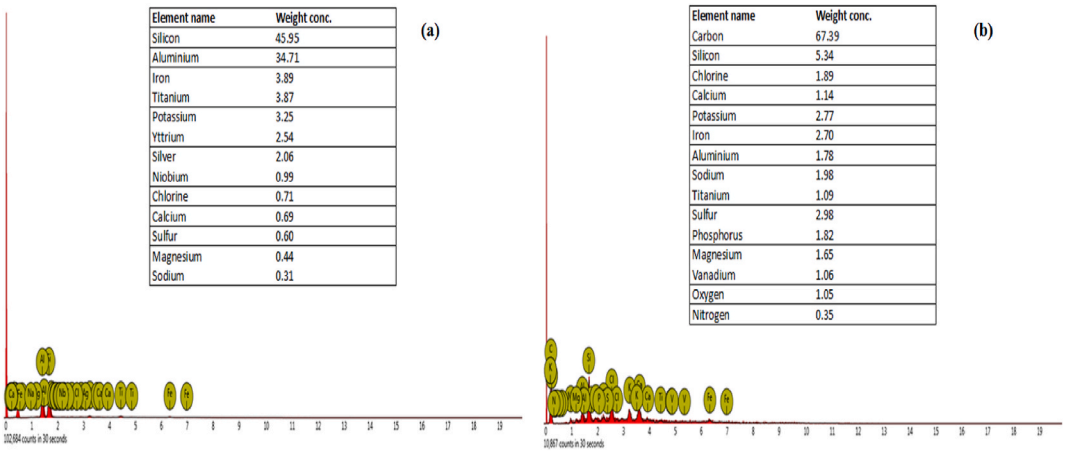

Element name	Weight conc.
Silicon	45.95
Aluminium	34.71
Iron	3.89
Titanium	3.87
Potassium	3.25
Yttrium	2.54
Silver	2.06
Niobium	0.99
Chlorine	0.71
Calcium	0.69
Sulfur	0.60
Magnesium	0.44
Sodium	0.31

Element name	Weight conc.
Carbon	67.39
Silicon	5.34
Chlorine	1.89
Calcium	1.14
Potassium	2.77
Iron	2.70
Aluminium	1.78
Sodium	1.98
Titanium	1.09
Sulfur	2.98
Phosphorus	1.82
Magnesium	1.65
Vanadium	1.06
Oxygen	1.05
Nitrogen	0.35

Fig. 4. EDX spectrum of (a) RLCF and (b) MLCF.

3. Results and discussion

3.1. Characterization of the adsorbents

The FITR spectra for RLCF and MLCF are shown in Fig. 2(a) and **(b)**, respectively. In the FTIR spectra of RLCF, the peak observed at 2972 cm^{-1} is attributed to the asymmetric and symmetric stretching vibrations of CH_2 (methylene) and CH_3 (methyl) groups [20]. Following the NaOH treatment, this peak diminishes, shifting to 2851 cm^{-1}. The presence of functional groups corresponding to carbonyl groups and aromatic C═C stretching is shown by the peaks at wavenumbers 2171 cm^{-1} and 1570 cm^{-1}, respectively. However, a substantial portion of the peak is located in the fingerprint region. Additionally, peaks at 1054 cm^{-1} and 1032 cm^{-1}, which undergo a shift to 1038 cm^{-1} post-modification, are linked to C–O stretching vibrations in alcohol. The occurrence of peaks in the range of 574–510 cm^{-1} indicates the presence of bending deformations in lignin and hemicellulose [26]. In the FTIR spectrum of MLCF, notable shifts are observed in some peaks. The peak at 3100 cm^{-1} implies aliphatic C–H stretching. Peaks at 1697 cm^{-1} and 1597 cm^{-1} are associated with C═C and C═O stretching in aromatic components, while the peak at 1169 cm^{-1} is attributed to the asymmetric C–O stretching of C–*O*–C in cellulose and hemicellulose [27].

The SEM images in Fig. 3 reveal the surface characteristics and structural features of RLCF and MLCF. In Fig. 3a, depicting the raw *Luffa cylindrica* fiber (RLCF), a smooth and uniform surface is evident. Upon modification, illustrated in Fig. 3b for MLCF, the morphology undergoes changes, revealing the formation of voids and crevices. The surface of MLCF becomes notably heterogeneous and rough, resulting in an interconnected porous structure with a hierarchical arrangement. This hierarchical porosity is ascribed to the elimination of silica during the modification process, as indicated by EDX analysis. The removal of silica facilitates the generation of pores and voids in MLCF [27]. The existence of voids is advantageous, providing ample binding sites for adsorbates during the adsorption process [28].

Fig. 4 illustrates the elemental composition of the adsorbents as determined by energy-dispersive X-ray spectroscopy (EDX). In Fig. 4a, the primary elements in RLCF are silicon and aluminum, with weight concentrations of 45.95% and 34.71%, respectively. This

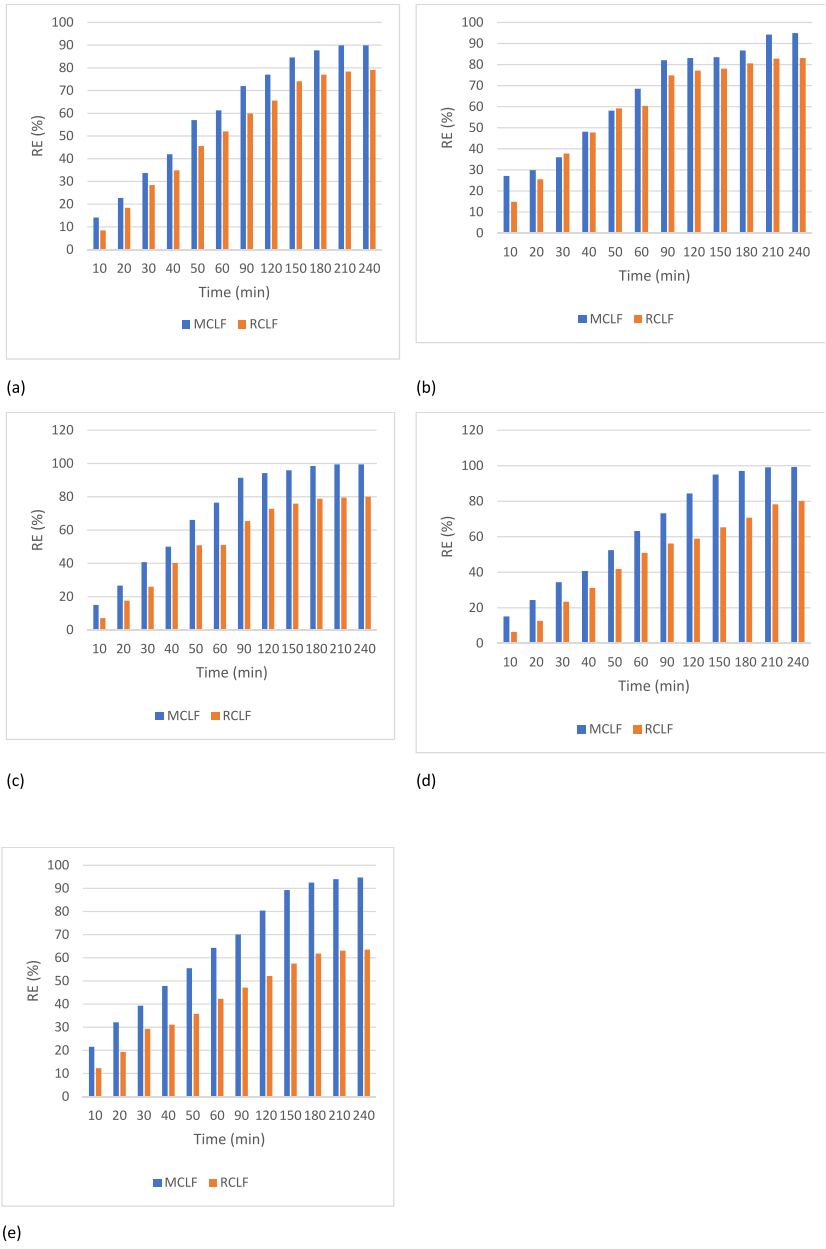

Fig. 5. Effect of time on % removal of **(a)** 100 **(b)** 200 **(c)** 300 **(d)** 400 **(e)** 500 mg/l of phenol.

indicates a significant amount of silicon and aluminum in RLCF, typical constituents found in natural fibers. The presence of silicon suggests the existence of minerals, potentially derived from the plant structure, while aluminum may be linked to the fibrous matrix. In MLCF (Fig. 4b), carbon dominates the composition with a weight concentration of 67.39%, indicating a significant presence of organic material in MLCF. This implies that the primary carbon-based component of plant fibers, cellulose, may have been exposed as a result of the NaOH treatment, which also may have eliminated some inorganic elements like silica and alumina. The results also indicate the presence of diverse elements in varying quantities, potentially influencing the overall physicochemical properties of both RLCF and MLCF and thereby affecting their adsorption capacity.

3.2. Optimization studies

3.2.1. The influence of contact time

To determine the optimum contact time to attain equilibrium, 13 g of RLCF and MLCF were combined with phenol in each packed bed at varying times (10–240 min). Fig. 5(a–**e**) illustrate the results, showing how the percentage of phenol removal by the adsorbents

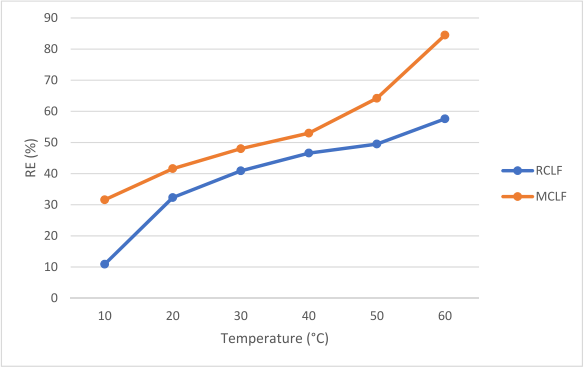

Fig. 6. Plot of temperature on phenol removal efficiency of RCLF and MCLF.

is influenced by contact time. The results indicate that the adsorption process removes phenol rapidly in the first 120 min. After that, the rate of adsorption slowed down until it reached equilibrium. This trend can be attributed to the fact that active sites were readily available for adsorption at the start of the process, but as the phenol molecules started to accumulate on the active sites, they gradually became occupied, leading to a decrease in the rate of adsorption [29]. The highest percentage removal at 100, 200, 300, 400, and 500 mg/L phenol concentrations for the RLCF were 79.1, 83.1, 80.0, 80.1, and 63.5%, while for the MLCF, they were 89.9, 94.9, 99.5, 99.3, and 94.7%, respectively. When compared to the RLCF, the MLCF had a greater adsorption capacity and percentage elimination.

3.2.2. The influence of temperature

The operating temperature is a crucial parameter that can affect the rate of adsorption in a positive or negative way. The set-up procedure was done at an initial phenol concentration of 300 mg/l, an adsorbent dosage of 13 g, and pH 7. It has been asserted that the adsorption process is endothermic when the percentage of phenol removed increases as the temperature rises [6]. This might be because when the temperature rises, there are more adsorption sites available and the phenol is more mobile [30]. Fig. 6 presents the analysis of the effect of temperature, ranging from 40 to 60 °C, on the removal efficiency of phenol using RLCF and MLCF. The findings indicate that a rise in temperature resulted in a greater removal percentage of phenol for both adsorbents. This suggests that the adsorption is an endothermic process. The highest removal efficiency of 57.6% and 84.5% were observed at 60 °C for the RLCF and MLCF, respectively.

3.3. Adsorption isotherm

The dispersion of phenol molecules between the aqueous mixture and the adsorbents in different packed beds of RLCF and MLCF was explained using different isotherm models. The plot of $\frac{C_e}{q_e}$ versus q_e (Fig. 7a), linear method was used to establish the Langmuir model using RLCF and MLCF packed beds. The Langmuir constants were obtained from the gradient $\frac{1}{q_m}$ and intercept $\frac{1}{q_m K_L}$ (Tables 1 and 2). The R^2 obtained for the RLCF-PB (0.0001–0.4385) and for the MLCF-PB (0.0199–0.9185) are comparably good for the modified packed bed but essentially low for the RLCF-PB. This indicates that adsorption to the RLCF-surface PB's is not monolayer [31]. The K_L (mg/g) and the equilibrium constant for RLCF-PB and MLCF-PB ranged from −0.0002–0.0757 mg/g and 0.0004−−0.0153 mg/g, respectively. The K_L values are proportional to the distribution's intensity, which describes the adsorbent-solute affinity [32].

The separation factor (R_L), ($0 < R_L < 1$), which gave a positive number, suggests that the adsorption experiment is feasible. The separation factors (R_L) values for MLCF-PB (0.2639–0.8509) and RLCF-PB (0.3321–1.3116) revealed that the procedure was beneficial since it fell between the agreeable range of 0 and 1 except for $R_L = 1.0851$ and 1.3116, which is slightly above 1 [33,34]. This indicates that phenol adsorption onto the MLCF-PB is very favorable, with a high level of irreversibility, as R_L approached the lower satisfactory range (close to zero).

For the Freundlich model (plot shown in Fig. 7b), the Freundlich exponent, n, is in the range of 1–2. This value indicates moderately good, suggesting the adsorption's favorability. Values of 2–10 for n indicate 'good,' while less than 1 indicates 'bad' adsorption characteristics [35]. The n values found in this study for MLCF-PB (1.0783–1.7221) were consistently moderate throughout the experiment (as shown in Table 2), while RLCF-PB has a mixture of 'poor' and "good" adsorption qualities (Table 1). The R^2 values for the Freundlich isotherm were generally high (ranging from 0.6866 to 0.9734) for both adsorbents, but with some lower values (ranging from 0.0193 to 0.9727) in comparison to the Langmuir model, which had R^2 values that ranged from 0.0199 to 0.9185 for RLCF and 0.0001 to 0.4385 for MLCF, respectively. This suggested that the Freundlich model rather than the Langmuir model better predicts phenol adsorption. The results show that as time passed, the adsorption intensity (K_F) values increased, which signifies that the chemical used for the modification of the packed bed has a substantial effect on the adsorbent [36].

The equilibrium-binding constant (A) of the Temkin isotherm (Fig. 7c) gave a set of positive values, which is favorable at equilibrium time [37]. It increased as contact time increased [38]. These heat of adsorption values B (J/mol) rose at the first 60 min of the experiment using the RLCF-PB, which later declined towards the end of the experiment, while the values increased as time increased for the MLCF-PB [39]. According to the Temkin isotherm, the R^2 values for RLCF-PB (0.0019–0.8976) and MLCF-PB (0.5280–0.9617)

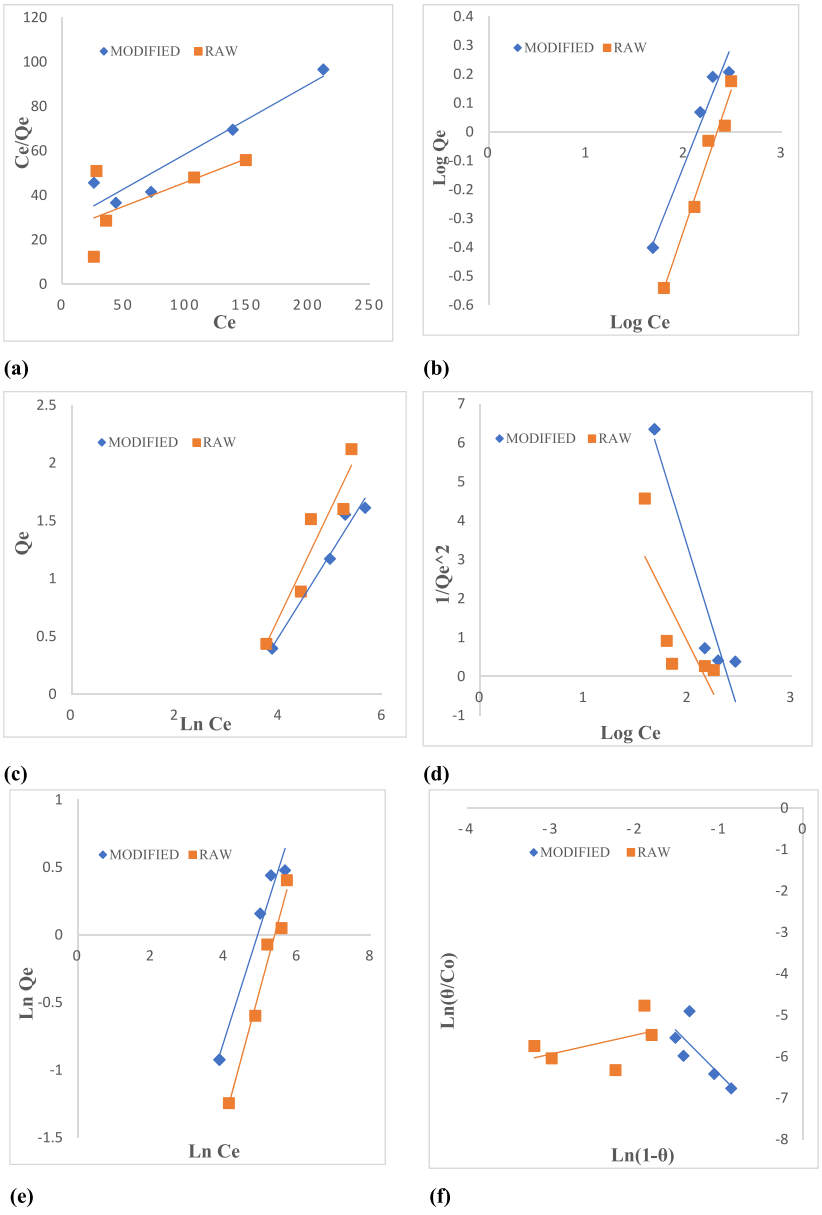

Fig. 7. Isotherm models for phenol adsorption on RLCF-PB and MLCF-PB. Langmuir (a), Freundlich (b), Temkin (c), Harkins-Jura (d), Halsey(e), Flory-Huggins (f) models.

were higher than those derived from the Langmuir isotherms, but they were lower than those from the Freundlich isotherm. This indicates that the Freundlich isotherm is a better model for explaining the adsorption behavior, suggesting that the modified packed bed is characterized by a multilayer surface structure [40].

The R^2 values obtained from the Harkins-Jura model (Fig. 7d) for MLCF-PB (0.9339) are superior to those for RLCF-PB (0.8730), but they are lower than those obtained from the Freundlich and Temkin models, indicating that the Harkins-Jura model is not the best fit for this experiment. The parameters A and B were estimated for both RLCF-PB and MLCF-PB, except for the negative values (−3.3636 and −2.5648) and (−1.1473 and −0.7063) obtained for A and B at 210 and 240 min, which may not be favorable at those specific times [41].

The large R^2 values (0.9339) of the Halsey isotherm (Fig. 7e) using the MLCF-PB compared to Langmuir and Temkin explain further why the Freundlich isotherm model well predicts phenol adsorption onto the MLCF-PB. The coverage of adsorbate on the adsorbent surface is typically described by the Flory-Huggins isotherm model (Fig. 7f). The model, however, showed the lowest correlation coefficient in the study ($R^2 = 0.2415$). The equilibrium constant for the Flory-Huggins model is denoted as K_{FH}. The suitability order of the models is Freundlich > Halsey > Temkin > Harkins-Jura > Langmuir > Flory Huggins. Table 3 compares the values of the different

Table 1
Isotherm model estimated parameters for RLCF-PB.

Isotherm	Parameters	Time											
		10	20	30	40	50	60	90	120	150	180	210	240
Langmuir	Q_m (mg/g)	−6.3251	−3.4602	250.00	344.83	7.9554	15.015	4.6512	9.1827	6.3939	3.5932	4.1305	3.8124
	K_L (mg/g)	−0.0002	−0.0007	0.0001	0.0001	0.0016	0.0011	0.0089	0.0052	0.0138	0.0477	0.0627	0.0757
	RL	1.0851	1.3116	0.9705	0.9745	0.7376	0.8357	0.4292	0.6624	0.5743	0.3599	0.3460	0.3321
	R^2	0.0109	0.2046	0.0003	0.0001	0.2483	0.0573	0.4385	0.0990	0.0827	0.2027	0.2190	0.2036
Freundlich	K_F (mg/g)	0.0014	0.0012	0.0046	0.0053	0.0172	0.0200	0.2022	0.2122	0.4235	1.4629	2.0114	2.1193
	1/n	1.0391	1.1594	1.0009	1.0391	0.8953	0.9421	0.5113	0.5651	0.4572	0.0855	−0.0302	−0.0576
	N	0.9624	0.8625	0.9991	0.9624	1.1169	1.0615	1.9558	1.7696	2.1872	11.695	−33.112	−17.361
	R^2	0.7753	0.9440	0.9727	0.9388	0.8963	0.8152	0.4213	0.3619	0.1633	0.0110	0.0026	0.0093
Temkin	A (L/mg)	0.0168	0.0159	0.0212	0.0239	0.0371	0.0439	0.1907	0.1908	0.4720	199.86	2.1E10	1.27E20
	B (J/mol)	0.3379	0.5804	0.6977	0.8639	0.9392	1.1566	0.7617	0.9723	0.8721	0.2698	0.0855	0.0459
	R^2	0.6816	0.8223	0.8954	0.8973	0.8976	0.8816	0.5300	0.4786	0.2121	0.0366	0.0069	0.0019
Harkins Jura	A	0.0092	0.0216	0.0604	0.0772	0.1554	0.1880	0.5144	0.5693	0.7179	6.2854	−3.3636	−2.5648
	B	2.5220	2.4651	2.4268	2.3547	2.2740	2.1665	2.1884	2.0365	1.8542	5.1709	−1.1473	−0.7063
	R^2	0.6740	0.7766	0.8730	0.7626	0.7476	0.6033	0.2551	0.2084	0.1384	0.0039	0.0284	0.0473
Halsey	K	570.41	325.18	217.43	155.13	93.569	63.467	22.799	15.539	6.5487	−85.552	8.9E-11	2.17E-6
	1/n	−1.0391	−1.1594	−1.0009	−1.0391	−0.8953	−0.9421	−0.5113	−0.5651	−0.4572	−0.0855	0.0302	0.0576
	R^2	0.7753	0.9440	0.9727	0.9388	0.8963	0.8152	0.4213	0.3619	0.1633	0.0110	0.0026	0.0093
Flory Huggins	K	3.78E-4	0.0034	0.0012	0.0033	0.0007	0.0029	0.0022	0.0046	0.0104	0.0081	0.0077	0.0084
	N	−2.8966	3.7879	−0.3543	1.0324	−1.2483	0.1248	−0.1873	0.1897	0.4577	0.2874	0.2095	0.2264
	R^2	0.1008	0.1285	0.0005	0.0157	0.0594	0.0016	0.0225	0.0286	0.2388	0.2109	0.2021	0.2415

Table 2
Isotherm model estimated parameters for MLCF-PB.

Isotherm	Parameters	Time (min)											
		10	20	30	40	50	60	90	120	150	180	210	240
Langmuir	Q_m (mg/g)	2.0227	1.4921	3.1358	2.6731	2.4178	4.8948	2.7847	2.9386	3.1980	3.5436	3.5361	3.4891
	K_L (mg/g)	0.0004	0.0015	0.0012	0.0023	0.0047	0.0019	0.0081	0.0097	0.0115	0.0119	0.0141	0.0153
	RL	0.8509	0.6228	0.7020	0.5579	0.3987	0.6458	0.3183	0.3008	0.2906	0.3057	0.2777	0.2639
	R^2	0.0199	0.2239	0.2282	0.4684	0.6850	0.7034	0.7605	0.8089	0.9185	0.9098	0.8685	0.8658
Freundlich	K_F (mg/g)	0.0012	0.0050	0.0074	0.0143	0.0333	0.0151	0.0792	0.0960	0.1044	0.1074	0.1138	0.1193
	1/n	0.9274	0.7992	0.8307	0.7713	0.6727	0.8535	0.5899	0.5807	0.5989	0.6224	0.6335	0.6301
	N	1.0783	1.2513	1.2038	1.2965	1.4865	1.1716	1.6952	1.7221	1.6697	1.6067	1.5785	1.5870
	R^2	0.6866	0.7785	0.8492	0.8096	0.7626	0.9734	0.7012	0.7187	0.8485	0.8609	0.8193	0.8011
Temkin	A (L/mg)	0.0158	0.0221	0.0240	0.0333	0.0548	0.0366	0.0839	0.1040	0.1020	0.1062	0.1158	0.1223
	B (J/mol)	0.1704	0.2665	0.4322	0.4797	0.5263	0.7196	0.6237	0.6691	0.7549	0.8350	0.8799	0.8818
	R^2	0.5280	0.6843	0.7907	0.9046	0.8792	0.9617	0.8377	0.8450	0.9425	0.9538	0.8921	0.8602
Harkins Jura	A	0.0033	0.0167	0.0399	0.0650	0.1242	0.1158	0.2568	0.3129	0.3734	0.3985	0.4142	0.4229
	B	2.5905	2.5649	2.5042	2.4589	2.4203	2.3859	2.3385	2.2937	2.2209	2.1599	2.1102	2.0953
	R^2	0.7052	0.7074	0.7133	0.6275	0.5779	0.9339	0.4871	0.5012	0.6303	0.6323	0.6034	0.5990
Halsey	K	1446.7	752.11	364.72	246.46	156.97	136.45	73.616	56.619	43.514	36.018	30.881	29.183
	1/n	−0.9274	−0.7992	−0.8307	−0.7713	−0.6727	−0.8535	−0.5899	−0.5807	−0.5989	−0.6224	−0.6335	−0.6301
	R^2	0.6866	0.7785	0.8492	0.8090	0.7626	0.9734	0.7012	0.7187	0.8485	0.8609	0.8193	0.8011
Flory Huggins	K	1.36E-4	1.34E-4	2.12E-4	2.75E-4	3.07E-4	7.08E-4	4.81E-4	4.58E-4	2.11E-4	1.97E-4	2.66E-4	3.06E-4
	N	−9.2764	−7.9489	−4.7788	−3.4809	−2.7315	−1.2845	−1.6239	−1.5449	−2.0467	−1.9422	−1.6186	−1.4950
	R^2	0.2560	0.3635	0.2802	0.3145	0.3985	0.3393	0.3775	0.3945	0.5961	0.5588	0.4337	0.3967

Table 3
Assessment of different adsorbents for the elimination of phenol from aqueous solution.

Adsorbent	n	Q_L	R_L	References
Raw *Luffa cylindrica* fiber	−33.112-11.695	−6.325-344.83	0.3321–1.3116	**This study**
NaOH-modified *Luffa cylindrica* fiber	1.0783–1.6952	1.4921–4.8948	0.2639–0.8509	**This study**
Unmodified mango seed shell AC	1.5506–1.6918	35.971–44.843	0.2851–0.4484	[42]
Nano-modified mango seed shell AC	1.1573–1.3385	−99.01 to 62.11	0.7276–1.2029	[42]
Organically modified manganite	NA	52.19	0.084	[43]
Modified Rhassoul (clay)	NA	25	0.022	[44]
Avocado kernel seed-activated carbon	4.73	0.215	9.4×10^{-5}	[45]

NA= Not Available.

Table 4
Parameters of kinetic models for phenol adsorption onto RLCF-PB.

Kinetics	Parameters	Concentration				
		100 mg/l	200 mg/l	300 mg/l	400 mg/l	500 mg/l
Pseudo 1st Order	Qe (mg/g)	0.4135	0.7108	1.3862	2.0127	1.8658
	K_1 (min^{-1})	0.0104	0.0121	0.0143	0.0095	0.0130
	R^2	0.2822	0.3572	0.4703	0.5511	0.5017
Pseudo 2nd Order	Qe (mg/g)	0.8802	1.6964	2.8019	4.0290	3.0516
	K_2 (mg/g.min^{-1})	0.0122	0.0082	0.0035	0.0017	0.0056
	R^2	0.9650	0.7889	0.8987	0.8777	0.9967
Elovich	α (mg/g min)	0.0227	0.0598	0.0701	0.0771	0.1145
	β (g/mg)	5.3562	2.7778	1.7094	1.3303	1.5058
	R^2	0.9868	0.8489	0.9739	0.9776	0.9904

Table 5
Parameters of kinetic models for phenol adsorption onto MLCF-PB.

Kinetics	Parameters	Concentration				
		100 mg/l	200 mg/l	300 mg/l	400 mg/l	500 mg/l
Pseudo 1st Order	Qe (mg/g)	0.2887	0.8716	1.0144	2.9411	2.8005
	K_1 (min^{-1})	0.0024	0.0099	0.0080	0.0170	0.0141
	R^2	0.0217	0.3500	0.1983	0.5319	0.5839
Pseudo 2nd Order	Qe (mg/g)	0.0163	1.7355	2.9994	4.3029	4.4903
	K_2 (mg/g.min^{-1})	0.0056	0.0120	0.0055	0.0027	0.0041
	R^2	0.9866	0.9851	0.9705	0.9865	0.9986
Elovich	α (mg/g min)	0.0299	0.0808	0.1076	0.1141	0.1821
	β (g/mg)	4.9505	2.6709	1.4560	1.0746	1.0248
	R^2	0.9809	0.9476	0.9499	0.9755	0.9946

models obtained in this study for the adsorption of phenol with other reported values.

3.4. Kinetics studies

The PFO, PSO, and Elovich models were utilized to investigate the kinetic studies and rate constants of phenol adsorption by RLCF-PB and MLCF-PB. The obtained kinetic constants and correlation coefficients (R^2) for phenol adsorption are provided in Tables 4 and 5. The values K_1 and q_e were obtained from the plots of $\ln(q_e - q_t)$ against t. The plot of the concentration (100–500 mg/l) for RLCF-PB and MLCF-PB showed a range of values for R^2. Based on the results, the PSO model was determined to be the best suitable kinetic model for explaining the adsorption process of phenol onto RLCF-PB and MLCF-PB. This is supported by the higher values of the correlation coefficient (R^2) and the agreement between the calculated and experimental adsorption capacities. This indicates that the adsorption rate is influenced by the availability of vacant binding sites [21]. The data obtained from the PFO model plots for both RLCF-PB and MLCF-PB did not fit well, indicating that the adsorption process did not conform to the PFO model. However, the plots for the PSO model showed a good fit, as depicted in Fig. 8(a–e), and the parameters K_2 and q_e for the PSO model were determined from the intercepts ($\frac{1}{K_2 q_e^2}$) and slopes ($\frac{1}{q_e}$) of the plots of $\frac{t}{q(t)}$ against t. It was found that PFO was only appropriate for the initial phase of the adsorption process, while PSO could accurately describe the entire range of adsorption contact time. PSO is considered a suitable model for describing adsorption processes that involve chemisorption, where strong chemical bonds are formed between the adsorbate and the adsorbent [46].

The PSO model showed R^2 values close to 1 for both RLCF-PB (0.9967) and MLCF-PB (0.9986), suggesting a strong fit of the model to the adsorption data. The adsorption rates measured for RLCF-PB and MLCF-PB in Tables 4 and 5 were relatively low, ranging from

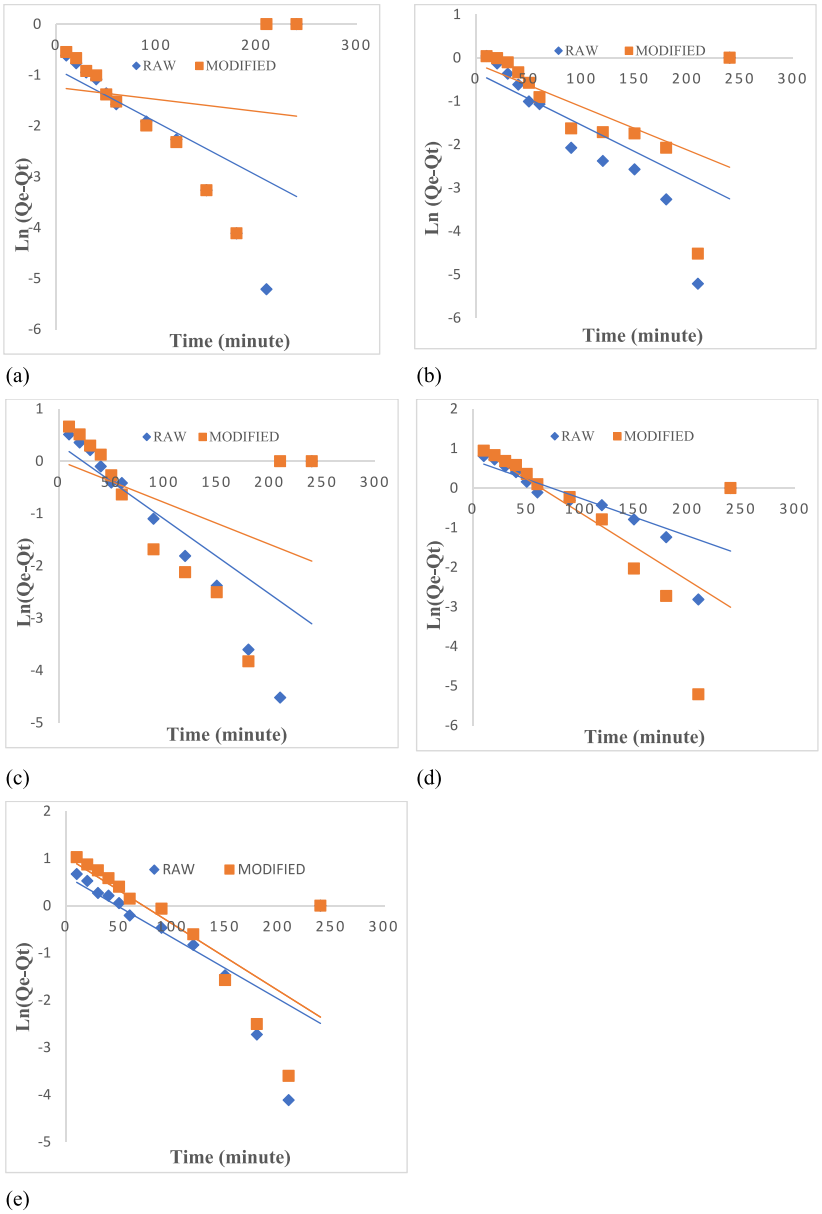

Fig. 8. Plot of $\ln(q_e - q_t)$ against t for phenol adsorption onto RLCF-PB and MLCF-PB at concentrations of **(a)** 100, **(b)** 200, **(c)** 300, **(d)** 400, and **(e)** 500 mg/l.

0.0017 to 0.0122 mg/g min for RLCF-PB and 0.0027–0.0120 mg/g min for MLCF-PB. These results imply that the adsorption process was chemisorption. Additionally, the Elovich model was used to gain a better understanding of the adsorption process, and the maximum R^2 values for RLCF-PB (0.9904) and MLCF-PB (0.9946) further supported the notion that phenol adsorption occurred via chemisorption. The plots for the Elovich model is shown in Fig. 9(a–e). PSO has also been reported as the best-fit kinetic model for phenol removal in previous studies by Mittal et al. [47], Kumar et al. [48], and El-Bery et al. [49], using agricultural materials such as deoiled soya, modified wood apple fruit shell, and activated sugarcane bagasse, respectively. The order of suitability for the models in this study was PSO > Elovich > PFO.

3.4.1. Error analysis for the kinetic models

The assessment of the kinetic models was performed based on the sum of squared errors (SSE, %) and average relative error, alongside the R^2 value. Table 6 presents the results of the error test for the first- and second-order models of phenol adsorption onto RLCF-PB and MLCF-PB. A higher R^2 and lower SSE values indicate a better model. The table demonstrates that the PSO model offers superior accuracy in predicting the adsorption kinetics of phenol onto RLCF-PB and MLCF-PB than the PFO model.

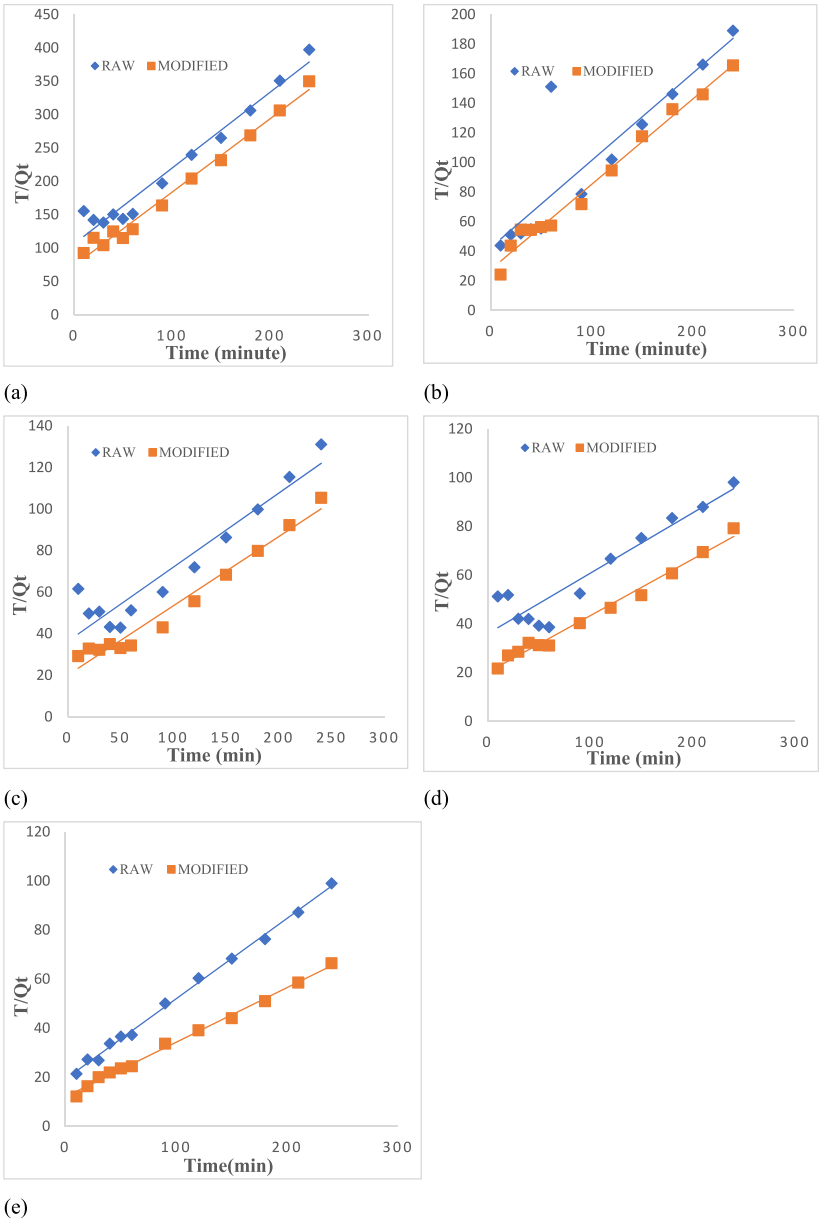

Fig. 9. Plot of log $\frac{t}{q(t)}$ against t for phenol adsorption onto RLCF-PB and MLCF-PB at concentrations of **(a)** 100, **(b)** 200, **(c)** 300, **(d)** 400, and **(e)** 500 mg/l.

3.5. Adsorption mechanism

The study investigated the possibility of intra-particle (Weber-Morris) diffusion and its effect on the rate of phenol adsorption onto packed beds. However, the plot did not touch some of the points during the experimental period, indicating that other factors influence the adsorption process [50]. As the intraparticle plots were extended up to the total duration of the experiment, which was 240 min, it was observed that the adsorption rate significantly decreased after the first 60 min as the system approached equilibrium over the next 120–240 min. Fig. 10 (a**–e)** showed that the MLCF-PB had a faster initial rate of phenol adsorption than at later stages. This can be explained by the fact that LCF molecules occupy the external sites and channels, while phenolic molecules diffuse through the inner apertures of the materials.

K_i were obtained from the gradients of the graphs of q_t against $t^{0.5}$ (shown in Fig. 10 (a–e). The intra-particle diffusion model was used to plot the graphs at various initial concentrations (100–500 mg/L), with the plot showing multilinearity. The value of the constant C for RLCF-PB (−0.2001-0.1695) indicated a weaker adsorbent compared to MLCF-PB (−0.0882-0.3221) as the concentrations rose from 100 to 500 mg/L (as shown in Table 7). The K_i values showed similar patterns, although the driving force of

Table 6
Values for SSE and ARE in kinetic models.

Kinetic model	Concentration (mg l^{-1})	Raw *Luffa cylindrica* fiber PB		Modified *Luffa cylindrica* fiber PB	
		SSE	ARE	SSE	ARE
Pseudo 1st Order	100	0.0030	2.6293	0.0131	4.8258
	200	0.0026	3.6671	0.0278	3.3217
	300	0.0165	2.0244	0.1331	4.6226
	400	0.0157	1.4793	0.0007	0.2458
	500	0.0261	1.9224	0.0551	1.8758
Pseudo 2nd Order	100	0.0064	3.8087	0.0374	4.1353
	200	0.0152	2.8032	0.0068	1.6456
	300	0.0786	4.4188	0.0434	2.6385
	400	0.2085	4.3870	0.1349	3.4989
	500	0.0327	2.1520	0.0640	2.0206

concentration always had an impact on K_i, which was activated by a higher concentration of adsorbate [50].

3.6. Thermodynamic studies

The positive ΔG° values presented in Table 8 for all three temperatures and contact times were obtained from the graph of $\ln K_d$ against $1/T$ indicate that the products possess more enthalpy than the reactants, which suggests that the adsorption process is not spontaneous. The fact that the adsorption rate reduces as temperature increases suggests that the process is exothermic [51]. Additionally, as the contact time increased, the ΔG° values for both the RLCF-PB and the MLCF-PB decreased, indicating that the adsorption process became more feasible and spontaneous. The RLCF-PB had a larger ΔG° value than the MLCF-PB, which suggests that adsorption on the RLCF-PB is more favorable. The rise in ΔG° values as temperature rises can be clarified by the increased degree of spontaneity, which facilitates adsorption at elevated temperatures [3].

The ΔH° values obtained for the RLCF-PB and MLCF-PB were both positive, ranging from 4130.8 to 30902.6 J/mol for the RLCF-PB and 7928.6–25335.3 kJ/mol for the MLCF-PB. This demonstrated that the process absorbed heat, which is naturally endothermic. The small values of ΔS° (−28.306 to 30.006 J/mol K) for RLCF-PB and (−13.197 to 49.557 J/mol) for MLCF-PB indicate that the level of disorderliness on the solute/solid surface decreased during adsorption.

4. Conclusion

The study investigated the use of raw and NaOH-modified *Luffa cylindrica* fibers for sequestrating phenol from wastewater. The adsorption efficiency of both types of fibers in packed beds under various conditions was tested. The findings revealed that the NaOH-modified fiber was more effective than the raw fiber, achieving a removal efficiency of 99.5% at a phenol concentration of 300 mg/L, compared to 83.1% for the raw fiber at a concentration of 200 mg/L. It was also observed that the adsorption process was endothermic, as the highest removal efficiencies were achieved at higher temperatures. The thermodynamic characteristics of the adsorption process indicated its spontaneity and viability. Various isotherm models were used to fit the equilibrium data, and it was found that the Freundlich model was the best fit. This suggested that phenol molecules formed a monolayer on the surface of the NaOH-modified fiber. The study also examined the kinetics of phenol adsorption and found that the PSO model was the best fit for the data. Overall, the study has shown that NaOH-modified *Luffa cylindrica* fiber in a packed bed could be a promising material for phenol removal from aqueous media. The adsorbent's advantages include its low cost, non-toxicity, high effectiveness, ease of use, and superficial synthesis and preparation.

Ethics approval and consent to participate

Not applicable.

Consent for publication

The authors have unanimously decided that this manuscript be sent for possible publication.

Consent to publish

Not applicable.

Compliance with ethical standards

This article does not contain any studies involving human or animal subjects.

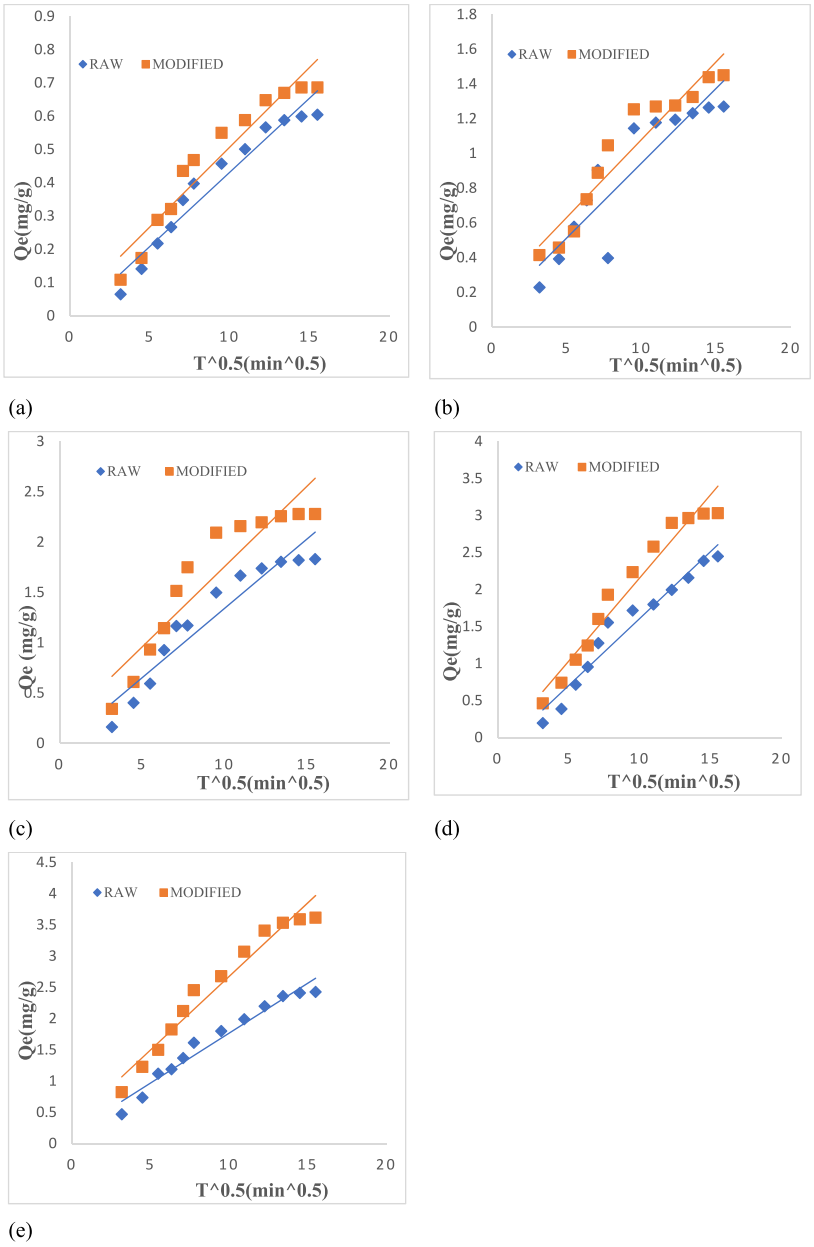

Fig. 10. Plot of q_t against $t^{0.5}$ for phenol adsorption onto RLCF-PB and MLCF-PB at concentrations of **(a)** 100, **(b)** 200, **(c)** 300, **(d)** 400, and **(e)** 500 mg/l.

Table 7
Intra-particle diffusion model parameters.

Conc. (mg/l)	Raw *Luffa cylindrica* fiber PB			NaOH- modified *Luffa cylindrica* PB		
	K_i	C	R^2	K_i	C	R^2
100	0.0446	−0.0141	0.9409	0.0479	0.0275	0.9249
200	0.0861	0.0833	0.8141	0.0896	0.1839	0.9097
300	0.1378	−0.0352	0.9045	0.1597	0.1610	0.8598
400	0.1811	−0.2001	0.9500	0.2249	−0.0882	0.9545
500	0.1598	0.1695	0.9503	0.2353	0.3221	0.9688

Table 8
Thermodynamic parameters for phenol adsorption onto RLCF-PB and MLCF-PB.

Time (min)	Temp. (K)	RLCF-PB			MLCF-PB		
		ΔS (J/molK)	ΔH (J/mol)	ΔG (J/mol)	ΔS (J/molK)	ΔH (J/mol)	ΔG (J/mol)
10	313	35.009	30902.3	−20004.9	−11.955	11613.8	−15389.3
	323			−19465.1			−15403.9
	333			−19312.7			−15632.8
20	313	9.3923	18589.3	−15720.3	−13.197	10017.5	−14167.8
	323			−15403.9			−14239.6
	333			−15541.9			−14434.3
30	313	0.4240	14653.4	−14523.9	−12.654	9543.6	−13465.7
	323			−14510.2			−13713.7
	333			−14515.9			−13713.6
40	313	−25.156	5455.9	−13364.6	−8.4952	10329.3	−12989.3
	323			−13507.1			−13071.5
	333			−13872.3			−13159.4
50	313	−28.306	4130.8	−12989.3	−11.748	7928.6	−11636.7
	323			−13276.2			−11657.3
	333			−13555.3			−11875.7
60	313	−15.319	7535.6	−12344.1	49.557	25335.3	−9801.2
	323			−12454.7			−9377.2
	333			−12652.3			−8807.1

Additional information

No additional information is available for this paper.

Funding statement

This research was supported by Researchers Supporting Project (RSPD2024R768), King Saud University, Riyadh, Saudi Arabia.

CRediT authorship contribution statement

Samuel Ogunniyi: Writing – review & editing, Writing – original draft, Validation, Methodology, Investigation, Formal analysis, Data curation. **Ebuka Chizitere Emenike:** Writing – review & editing, Writing – original draft, Validation, Investigation, Data curation. **Kingsley O. Iwuozor:** Writing – review & editing, Writing – original draft, Validation. **Joshua O. Ighalo:** Writing – review & editing, Writing – original draft, Validation. **Abdelrahman O. Ezzat:** Writing – review & editing, Writing – original draft, Validation, Investigation, Funding acquisition. **Tunmise Latifat Adewoye:** Writing – review & editing, Writing – original draft, Validation. **Abel Egbemhenghe:** Writing – review & editing, Writing – original draft, Validation. **Hussein K. Okoro:** Writing – review & editing, Writing – original draft, Validation, Supervision. **Adewale George Adeniyi:** Writing – review & editing, Writing – original draft, Validation, Supervision, Project administration, Methodology, Investigation, Formal analysis, Conceptualization.

Declaration of competing interest

The authors declare that they have no known competing financial interests or personal relationships that could have appeared to influence the work reported in this paper.

Acknowledgment

The authors acknowledge the financial support through Researchers Supporting Project number (RSPD2024R768), King Saud University, Riyadh, Saudi Arabia.

References

[1] E.C. Emenike, J. Adeleke, K.O. Iwuozor, S. Ogunniyi, C.A. Adeyanju, V.T. Amusa, H.K. Okoro, A.G. Adeniyi, Adsorption of crude oil from aqueous solution: a review, J. Water Proc. Eng. 50 (2022) 103330.

[2] P. Adwani, J. Singh, Production of biochar from different feedstocks using various methods and its application for the reduction of environmental contaminants: a review, J.Appl. Sci. Innov. Technol. 2 (1) (2023) 18–24.

[3] K. Iwuozor, E. Emenike, F. Gbadamosi, J. Ighalo, G. Umenweke, F. Iwuchukwu, C. Nwakire, C. Igwegbe, Adsorption of organophosphate pesticides from aqueous solution: a review of recent advances, Int. J. Environ. Sci. Technol. (2022) 1–50.

[4] O. Ogunlalu, I.P. Oyekunle, K.O. Iwuozor, A.D. Aderibigbe, E.C. Emenike, Trends in the mitigation of heavy metal ions from aqueous solutions using unmodified and chemically-modified agricultural waste adsorbents, Current Research in Green and Sustainable Chemistry 4 (2021) 100188.

[5] E.C. Emenike, A.G. Adeniyi, K.O. Iwuozor, C.J. Okorie, A.U. Egbemhenghe, P.E. Omuku, K.C. Okwu, O.D. Saliu, A critical review on the removal of mercury (Hg2+) from aqueous solution using nanoadsorbents, Environ. Nanotechnol. Monit. Manag. (2023) 100816.

[6] O. Abdelwahab, N. Amin, Adsorption of phenol from aqueous solutions by Luffa cylindrica fibers: kinetics, isotherm and thermodynamic studies, The Egyptian Journal of Aquatic Research 39 (4) (2013) 215–223.
[7] A. Othmani, A. Kesraoui, M. Seffen, Removal of phenol from aqueous solution by coupling alternating current with biosorption, Environ. Sci. Pollut. Control Ser. 28 (2021) 46488–46503.
[8] C. Eryılmaz, A. Genc, Review of treatment technologies for the removal of phenol from wastewaters, J. Water Chem. Technol. 43 (2) (2021) 145–154.
[9] E.C. Emenike, S. Ogunniyi, J.O. Ighalo, K.O. Iwuozor, H.K. Okoro, A.G. Adeniyi, Delonix regia biochar potential in removing phenol from industrial wastewater, Bioresour. Technol. Rep. 19 (2022) 101195.
[10] F.A. Tomás-Barberán, J.C. Espín, Effect of food structure and processing on (Poly) phenol–gut microbiota interactions and the effects on human health, Annu. Rev. Food Sci. Technol. 10 (2019) 221–238.
[11] C.E. Iglesias-Aguirre, A. Cortés-Martín, M.Á. Ávila-Gálvez, J.A. Giménez-Bastida, M.V. Selma, A. González-Sarrías, J.C. Espín, Main drivers of (poly) phenol effects on human health: metabolite production and/or gut microbiota-associated metabotypes? Food Funct. 12 (21) (2021) 10324–10355.
[12] L.S. Yadav, B.K. Mishra, A. Kumar, S. Rawat, Treatment of phenolic wastewaters by mass transfer using crab eye surface modified adsorbent, J.Appl. Sci. Innov. Technol. 1 (2) (2022) 27–32.
[13] K.O. Iwuozor, J.O. Ighalo, E.C. Emenike, L.A. Ogunfowora, C.A. Igwegbe, Adsorption of methyl orange: a review on adsorbent performance, Current Research in Green and Sustainable Chemistry 4 (2021) 100179.
[14] E.C. Emenike, K.O. Iwuozor, S.U. Anidiobi, Heavy metal pollution in aquaculture: sources, impacts and mitigation techniques, Biol. Trace Elem. Res. (2021) 1–17.
[15] A.G. Adeniyi, J.O. Ighalo, Biosorption of pollutants by plant leaves: an empirical review, J. Environ. Chem. Eng. 7 (3) (2019) 103100.
[16] J.O. Ighalo, A.G. Adeniyi, O.A. Eletta, N.I. Ojetimi, O.J. Ajala, Evaluation of Luffa cylindrica fibres in a biomass packed bed for the treatment of fish pond effluent before environmental release, Sustainable Water Resources Management 6 (6) (2020) 120.
[17] M. Salimi, Z. Salehi, H. Heidari, F. Vahabzadeh, Production of activated biochar from Luffa cylindrica and its application for adsorption of 4-Nitrophenol, J. Environ. Chem. Eng. 9 (4) (2021) 105403.
[18] A.A. Oun, K.H. Kamal, K. Farroh, E.F. Ali, M.A. Hassan, Development of fast and high-efficiency sponge-gourd fibers (Luffa cylindrica)/hydroxyapatite composites for removal of lead and methylene blue, Arab. J. Chem. 14 (8) (2021) 103281.
[19] A. Adewuyi, F.V. Pereira, Underutilized Luffa cylindrica sponge: a local bio-adsorbent for the removal of Pb (II) pollutant from water system, Beni-Suef University journal of basic and applied sciences 6 (2) (2017) 118–126.
[20] C. Ye, N. Hu, Z. Wang, Experimental investigation of Luffa cylindrica as a natural sorbent material for the removal of a cationic surfactant, J. Taiwan Inst. Chem. Eng. 44 (1) (2013) 74–80.
[21] I. Anastopoulos, I. Pashalidis, The application of oxidized carbon derived from Luffa cylindrica for caffeine removal. Equilibrium, thermodynamic, kinetic and mechanistic analysis, J. Mol. Liq. 296 (2019) 112078.
[22] E.C. Emenike, K.O. Iwuozor, J.O. Ighalo, J.O. Bamigbola, E.O. Omonayin, H.T. Ojo, J. Adeleke, A.G. Adeniyi, Advancing the circular economy through the thermochemical conversion of waste to biochar: a review on sawdust waste-derived fuel, Biofuels (2023) 1–15.
[23] E.C. Emenike, H.K. Okoro, A.G. Adeniyi, K.O. Iwuozor, C. Zvinowanda, J.C. Ngila, Applications of bean pod and husk for remediation of water contamination: a review, Bioresour. Technol. Rep. (2023) 101754, https://doi.org/10.1016/j.biteb.2023.101754.
[24] K.O. Iwuozor, C.T. Umeh, S.S. Emmanuel, E.C. Emenike, A.U. Egbemhenghe, O.T. Ore, T.T. Micheal, F.O. Omoarukhe, P.A. Sagboye, V.E. Ojukwu, A comprehensive review on the sequestration of dyes from aqueous media using maize-/corn-based adsorbents, Water Pract. Technol. (2023) wpt2023214.
[25] J.O. Ighalo, A.G. Adeniyi, E.O. Oke, L.T. Adewoye, F.O. Motolani, Evaluation of luffa cylindrica fibers in a biomass packed bed for the treatment of paint industry effluent before environmental release, European Journal of Sustainable Development Research 4 (4) (2020) em0132.
[26] E.C. Emenike, K.O. Iwuozor, S.A. Agbana, K.S. Otoikhian, A.G. Adeniyi, Efficient recycling of disposable face masks via co-carbonization with waste biomass: a pathway to a cleaner environment, Cleaner Environmental Systems 6 (2022) 100094.
[27] D.V. Cuong, C.-H. Hou, Engineered biochar prepared using a self-template coupled with physicochemical activation for highly efficient adsorption of crystal violet, J. Taiwan Inst. Chem. Eng. 139 (2022) 104533.
[28] E.C. Emenike, V.T. Amusa, K.O. Iwuozor, T. Ojeyemi, T.T. Micheal, K.T. Micheal, A.G. Adeniyi, Enhancing biochar properties through doping: a comparative study of sugarcane bagasse and chicken feather, Biofuels (2023) 1–8.
[29] E.C. Emenike, A.G. Adeniyi, P.E. Omuku, K.C. Okwu, K.O. Iwuozor, Recent advances in nano-adsorbents for the sequestration of copper from water, J. Water Proc. Eng. 47 (2022) 102715.
[30] S. Senthilkumaar, P. Kalaamani, C. Subburaam, Liquid phase adsorption of crystal violet onto activated carbons derived from male flowers of coconut tree, J. Hazard Mater. 136 (3) (2006) 800–808.
[31] A. Amole, D. Araromi, A. Alade, T. Afolabi, V. Adeyi, Biosorptive removal of nitrophenol from aqueous solution using ZnCl2-modified groundnut shell: optimization, equilibrium, kinetic, and thermodynamic studies, Int. J. Environ. Sci. Technol. 18 (7) (2021) 1859–1876.
[32] A.O. Alade, A.O. Arinkoola, T.J. Afolabi, A.A. Adegbola, D-OPTIMAL optimization of MICROWAVEASSISTED synthesis of moringa oleifera pod activated carbon and application to methylene blue adsorption, Annals of the Faculty of Engineering Hunedoara-International Journal of Engineering 3 (2020).
[33] N. Ayawei, A.N. Ebelegi, D. Wankasi, Modelling and interpretation of adsorption isotherms, J. Chem. (2017), 2017.
[34] D.H.K. Reddy, K. Seshaiah, A. Reddy, S. Lee, Optimization of Cd (II), Cu (II) and Ni (II) biosorption by chemically modified Moringa oleifera leaves powder, Carbohydr. Polym. 88 (3) (2012) 1077–1086.
[35] N.S. Kumar, M. Asif, M.I. Al-Hazzaa, A.A. Ibrahim, Biosorption of 2,4,6-trichlorophenol from aqueous medium using agro-waste: pine (pinus densiflora sieb) bark powder, Acta Chim. Slov. 65 (2018) 221–230, https://doi.org/10.17344/acsi.2017.3886.
[36] S. Veli, B. Aly, Adsorption of copper and zinc from aqueous solutions by using natural clay, J. Hazard Mater. 149 (2007) 226–233, https://doi.org/10.1016/j.jhazmat.2007.04.109.
[37] T. Karthikeyan, S. Rajgopal, L.R. Miranda, Chromium (VI) adsorption from aqueous solution by Hevea brasilinesis sawdust activated carbon, J. Hazard Mater. 124 (3) (2005) 192–199.
[38] P.S. Kumar, K. Kirthika, Equilibrium and kinetic study of adsorption of nickel from aqueous solution onto bael tree leaf powder, J. Eng. Sci. Technol. 4 (4) (2009) 351–363.
[39] S. Veli, B. Alyüz, Adsorption of copper and zinc from aqueous solutions by using natural clay, J. Hazard Mater. 149 (1) (2007) 226–233.
[40] A. Das, A. Bhowal, S. Datta, Biomass characterisation and adsorption mechanism of Cu (II) biosorption onto fish (Catla catla) scales, Int. J. Environ. Eng. 8 (1) (2016) 81–94, https://doi.org/10.1504/IJEE.2016.078242.
[41] F.O. Erdogan, Freundlich, Langmuir, Temkin, DR and Harkins-Jura isotherm studies on the adsorption of CO2 on various porous adsorbents, Int. J. Chem. React. Eng. 17 (5) (2019).
[42] I.O. Okeowo, E.O. Balogun, A.J. Ademola, A.O. Alade, T.J. Afolabi, E.O. Dada, A.G. Farombi, Adsorption of phenol from wastewater using microwave-assisted Ag–Au nanoparticle-modified mango seed shell-activated carbon, Int. J. Environ. Res. 14 (2) (2020) 215–233.
[43] M. Ge, X. Wang, M. Du, G. Liang, G. Hu, J.A. Sm, Adsorption analyses of phenol from aqueous solutions using magadiite modified with organo-functional groups: kinetic and equilibrium studies, Materials 12 (1) (2019) 96.
[44] M. Hamdaoui, M. Hadri, Z. Bencheqroun, K. Draoui, M. Nawdali, H. Zaitan, A. Barhoun, Improvement of phenol removal from aqueous medium by adsorption on organically functionalized Moroccan stevensite, J. Mater. Environ. Sci. 9 (4) (2018) 1119–1128.
[45] D. Kassahun, S. Khalid, A. Shimeles, Kinetic and thermodynamic study of phenol removal from water using activated carbon synthesizes from avocado kernel seed, Int. Lett. Nat. Sci. 54 (2016).
[46] K.O. Iwuozor, T.A. Abdullahi, L.A. Ogunfowora, E.C. Emenike, I.P. Oyekunle, F.A. Gbadamosi, J.O. Ighalo, Mitigation of levofloxacin from aqueous media by adsorption: a review, Sustainable Water Resources Management 7 (2021) 1–18.

[47] A. Mittal, D. Kaur, A. Malviya, J. Mittal, V. Gupta, Adsorption studies on the removal of coloring agent phenol red from wastewater using waste materials as adsorbents, J. Colloid Interface Sci. 337 (2) (2009) 345–354.
[48] N.S. Kumar, H.M. Shaikh, M. Asif, E.H. Al-Ghurabi, Engineered biochar from wood apple shell waste for high-efficient removal of toxic phenolic compounds in wastewater, Sci. Rep. 11 (1) (2021) 2586.
[49] H.M. El-Bery, M. Saleh, R.A. El-Gendy, M.R. Saleh, S.M. Thabet, High adsorption capacity of phenol and methylene blue using activated carbon derived from lignocellulosic agriculture wastes, Sci. Rep. 12 (1) (2022) 5499.
[50] A.E. Ofomaja, E.B. Naidoo, A. Pholosi, Intraparticle diffusion of Cr (VI) through biomass and magnetite coated biomass: a comparative kinetic and diffusion study, S. Afr. J. Chem. Eng. 32 (1) (2020) 39–55.
[51] N.A. Mohammed, R.A. Abu-Zurayk, I. Hamadneh, A.H. Al-Dujaili, Phenol adsorption on biochar prepared from the pine fruit shells: equilibrium, kinetic and thermodynamics studies, J. Environ. Manag. 226 (2018) 377–385.